Title: Magnetoimpedance effect in amorphous and nanocrystalline alloys based on iron

Author: Piotr Kwapuliński, Grzegorz Haneczok, Zbigniew Stokłosa, Józef Rasek

Journal of Achievements in Materials and Manufacturing Engineering
VOLUME 47
ISSUE 2
August
2011

Magnetoimpedance effect in amorphous and nanocrystalline alloys based on iron

P. Kwapuliński*, G. Haneczok, Z. Stokłosa, J. Rasek
Institute of Materials Sciences, University of Silesia,
ul. Bankowa 12, 40-007 Katowice, Poland
* Corresponding author: E-mail address: pkwapuli@us.edu.pl

Received 14.06.2011; published in revised form 01.08.2011

Properties

ABSTRACT

Purpose: The main purpose of the paper is to study magnetic, electrical and plastic properties of the selected group of amorphous alloys in the context of their application as magnetoimpedance sensors.
Design/methodology/approach: The presented results were obtained by applying different magnetic methods (low field permeability measurements, magnetic relaxation, magnetization versus magnetic field, magnetization in saturation versus temperature, magnetoimpedance effect versus static magnetic field and/or frequency), resistivity versus temperature and Young's modulus versus temperatures. Structural changes taking place in annealed samples were examined by making use of X-ray diffraction method and high resolution electron microscopy observations.
Findings: It was shown that in all examined amorphous alloys soft magnetic properties can be enhanced by applying a suitable 1-h annealing at temperatures T_{op} listed in Table 1. After annealing at this characteristic temperature magnetic permeability in relation to the as quenched state increases more than 20 times and non-contact magnetoimpedance effect $(\Delta Z/Z)^{nc}_{max}$ is of the order of 10^4%. This effect can be explained based on the random anisotropy model supplemented by energy terms describing magnetoelastic energy and stabilization energy related to free volume content. For the alloys for which the optimized microstructure corresponds to the relaxed amorphous phase the plastic deformation corresponding to formation of brittle cracks is much higher than for the examined nanostructured alloys. In the frequency range from 700 kHz to 2 MHz magnetoimpedenace effect $(\Delta Z/Z)^{nc}_{max}$ is approximately constant.
Research limitations/implications: Searching of new soft magnetic materials in the group of amorphous alloys based on iron obtained by melt spinning can give a promising result. For example one can obtain very good soft magnets showing also good mechanical properties.
Practical implications: Based on the presented results one can obtain very good soft magnetic material with low field relative magnetic permeability of about 16 000 ($Fe_{74}Cu_1Zr_3Si_{13}B_9$). In the examined group of amorphous alloys the best candidate for magnetoimpedane sensor applications is the $Fe_{75,75}Ag_{0,25}Nb_2B_{22}$ alloy for which $(\Delta Z/Z)^{nc}_{max} = 10^4$% and plastic deformation ε^{op}=0.015. Silver as an alloying addition to the base Fe-Nb-B alloy significantly improves the alloy plasticity.
Originality/value: It was shown that the examined amorphous alloys based on iron after applying a suitable thermal annealing can be used as promising materials for nagnetoimpedance sensors.
Keywords: Magnetoimpedance effect; Amorphous alloys; Magnetic permeability; Relaxed amorphous phase; Nanomagnets

Reference to this paper should be given in the following way:
P. Kwapuliński, G. Haneczok, Z. Stokłosa, J. Rasek, Magnetoimpedance effect in amorphous and nanocrystalline alloys based on iron, Journal of Achievements in Materials and Manufacturing Engineering 47/2 (2011) 166-176.

1. Introduction

The observed development of modern technologies requires new materials showing special functional properties [1]. In this context magnetic iron based amorphous and nanocrystalline alloys are of increasing interest as new promising and relatively cheap soft magnets. Indeed, low field magnetic permeability of these materials can be of the order of 10^4 with coercive field below 1 A/m and high resistivity of the order of $10^{-6}\Omega$m. The latter is important for soft magnets because it ensures low eddy current losses. The listed above parameters indicate a variety of industrial applications like core transformers, magnetic sensors, micro-generators or magnetic and electromagnetic shields etc. [2-5]. Especially interesting from practical and scientific point of view is the so-called magnetoimpedance effect which is of use in different kind of sensors [6-13]. For example magnetic sensors [7,8,12,14], stress sensors (giant stress impedance effect [15]), recording heads in hard discs [16] or biosensor systems (cancer cell detector) [12,17-19].

Amorphous alloys are frequently fabricated by applying the so-called melt spinning technique i.e. by fast cooling from liquid phase. In this case the obtained material is usually in form of ribbons with thickness and width of about 20-25 μm and 1 cm, respectively. These melt spun ribbons are frequently used as precursors of nanocrystalline alloys. Indeed, a well controlled annealing of amorphous alloy at higher temperatures may lead to crystallization (nanocrystallization) or a partial crystallization and in this way one can obtain different nanocrystalline materials with iron grains embedded into residual amorphous matrix [20-23]. It is proper to add that formation of nanocrystallites in an amorphous solid of an appropriate chemical composition requires controlling the annealing temperature and time to ensure relatively high nucleation rate and a small growth rate.

In general, magnetic properties of melt-spun amorphous ribbons strongly depend on chemical composition of a given alloy, preliminary thermal treatments and also the cooling rate has been applied in fabrication procedure. Nowadays different groups of amorphous and nanocrystalline alloys are still examined - i.e. *finemet* (like Fe-X-Si-B-Cu), *nanoperm* (Fe-X-B, Fe-X-B-Cu) or *hitperm* (Fe-Co-X-B-Cu) (X=alloying addition). The highest value of magnetic permeability is observed for *finemet* and *nanoperm* alloys, but the latter revels higher value of magnetization B_S (1-1.5 T) and relatively low Curie temperature T_c (300-400 K). Partially replacing of iron atoms by cobalt (*hitperm*) leads to an increase of B_S (>2 T) as well as T_C (>600 K) but causes also a decrease of permeability. Recently other groups based on Co or Ni - like Co-Fe-Si-B or Co-Ni-Si-B are also examined.

An interesting phenomenon observed in soft magnetic amorphous melt spun ribbons, is the so-called optimization effect. In fact, soft magnetic properties (magnetic permeability, coercive field) of these materials can be significantly enhanced by applying a suitable thermal annealing at temperatures closed to the crystallization temperature. In many papers (e.g., [4, 22-24]) it was shown that the optimization annealing causes an increase of magnetic permeability even more than 20 times. Moreover, this effect is correlated with a decrease of coercive field, resistivity and a reduction of thermal instabilities a characteristic feature of the as quenched state.

The optimization effect is usually explained by formation of iron nanocrystallites embedded in amorphous phase. According to the random anisotropy model [25] such a structure with grains of dimensions much smaller than the ferromagnetic exchange length gives a random distribution of magnetic anisotropy and leads to an enhancement of soft magnetic properties. Irrespective of this two other mechanisms are also taken into account: i) annealing out of free volume frozen into material during fast cooling from liquid phase which may lead to formation of small iron clusters and ii) a significant decrease of magnetostriction coefficient and internal stresses which reduces magnetoelastic energy.

In a series of paper [4,22-24,26,27] it was shown that the enhancement of magnetic permeability effect can be observed in samples free of iron nanograins. In this case the optimized microstructure corresponds to the so-called relaxed amorphous phase i.e. amorphous phase for which free volume content and internal stresses in relation to the as quenched state are significantly reduced. From practical point of view this effect seems to be of great importance because the relaxed amorphous phase does not show an increase of brittleness the main disadvantage of nanostructured magnets.

The aim of the present paper is to present and discuss in detail magnetic properties of a well selected group of iron based amorphous and nanocrystalline alloys in the context of some applications based on the magnetoimpedance effect.

2. Experimental

The experiments were carried out for the following amorphous alloys: $Fe_{76}Nb_2Si_{13}B_9$, $Fe_{75,75}Ag_{0,25}Nb_2Si_{13}B_9$, $Fe_{74}Cu_1Zr_3Si_{13}B_9$, $Fe_{75.75}Ag_{0.25}Nb_2B_{22}$, $Fe_{74}Co_5Cu_1Nb_2B_{18}$, $Fe_{74.75}Co_5Ag_{0.25}Nb_2B_{18}$ obtained by melt spinning technique in the form of ribbons with width and thickness of about 1 cm and 20-25 μm, respectively.

As quenched samples were annealed in vacuum for one hour at temperatures T_a ranging from 300 K to 1000 K (step 25 K). For the annealed samples at room temperature the following physical properties were measured:

i) low-field relative magnetic permeability μ_r (Maxwell-Wien bridge and Agilent meter E 4980a; H=0.5 A/m, frequency 1 kHz),
ii) intensity of magnetic relaxation $\Delta\mu_r/\mu_r$ (where $\Delta\mu_r/\mu_r=\frac{\mu_r(t_1)-\mu_r(t_2)}{\mu_r(t_1)}$, $\mu_r(t)$ is the magnetic permeability measured at time t_1=30 s and t_2=1800 s after demagnetization),
iii) magnetization curves, i.e. magnetization versus magnetic field (Lake Shore fluxmeter and/or magnetometer PPMS-7 Quantum Design),
iv) resistivity (four points probe),
v) plastic deformation $\varepsilon = d/2r$ (where d is the ribbon thickness and r is the bending radius corresponding to formation of the first brittle cracks),
vi) parallel magnetostriction coefficient $\lambda_{||S}$ at saturation magnetic field 0.1 T (infrared sensor dilatometer),
vii) magnetoimpedance effect $\Delta Z/Z$ using contact and non-contact methods (detail of measurement procedure are presented below).

Structural examinations were carried out by applying X-ray methods (X'Pert PW 3040/60 diffractometer, CuK_α line $\lambda = 0.1542$ nm) and high resolution electron microscopy observations (JEM 3010B).

As quenched samples were also examined using the so-called "in situ" measurements with linear heating rate ranging from 0.5 K/min to 10 K/min. In this way the following curves were determined: resistivity versus temperature (four points probe), magnetization in saturation versus temperature (magnetic balance) and Young's modulus E versus temperature (vibrating reed technique).

The idea of measurement of contact and non-contact magnetoimpedance effect is shown in Figs. 1 and 2, respectively. The tested sample is placed in static magnetic field H_{dc} and ac impedance is measured in two ways: i) for the contact method - the sample is directly connected to ac power source (the ac magnetic field H_{ac} is perpendicular to H_{dc}) or ii) for the non-contact method the sample is placed into magnetic coil connected to ac power source (the ac magnetic field H_{ac} is parallel to H_{dc}).

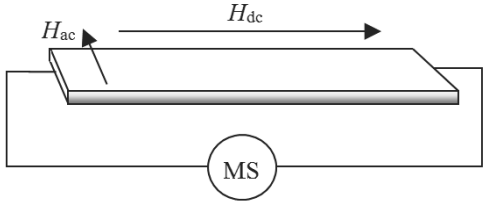

Fig. 1. Schematic diagram for con tact magnetoimpedance effect measurements; MS - measurement system

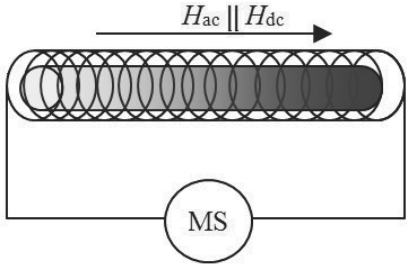

Fig. 2. Schematic diagram for non-contact magnetoimpedance effect measurements; MS - measurement system

Assuming that the impedance of a given magnetic coil is defined as:

$$Z = R_{ac} + jX \tag{1}$$

where R_{ac} is the resistance and X is the reactance (j^2=-1) one can define the magnetoimpedance effect as:

$$\Delta Z/Z = [|Z(H_{dc})| - |Z(H_{dc\,max})|]/|Z(H_{dc\,max})| \cdot 100\% \tag{2}$$

According to (2) the $\Delta Z/Z$ effect describes a relative change of magnetic impedance due to a change of static magnetic field from H_{dc} to $H_{dc\,max}$. If H_{dc}=0 and $H_{dc\,max}$ is the saturation field the magnetoimpedance effect is usually denoted as $(\Delta Z/Z)_{max}$. In the present paper we have used H_{dc}=0 and $H_{dc\,max}$=2900 A/m (the saturation field). It is proper to add that the non-contact method ensures that the examined sample is not subjected to any external deformations while in the case contact method because of sample grips such deformation is unavoidable.

The magnetoimpedance sensitivity ξ is defined as:

$$\xi = 2\,(\Delta Z/Z)_{max} / \Delta H_{dc} \tag{3}$$

where ΔH_{dc} is the half-width of the curve $\Delta Z/Z = f(H_{dc})$.

3. Results

3.1. Magnetic, electrical and mechanical properties

The examined alloys in the as quenched state were in amorphous state what is documented in Fig. 3 where as an example X-ray diffraction pattern and HREM image for the $Fe_{76}Nb_2Si_{13}B_9$ alloy are presented.

a)

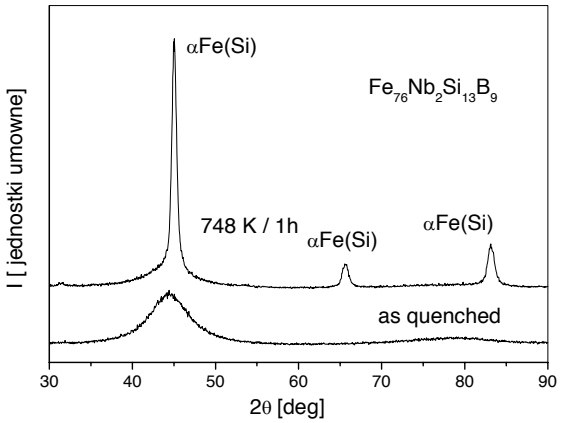

b)

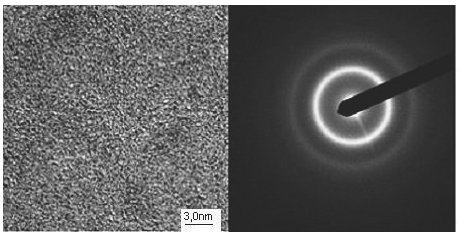

Fig. 3. a) X-ray diffraction pattern obtained for the $Fe_{76}Nb_2Si_{13}B_9$ alloy in the as quenched state and after annealing at 748/1h, b) HREM image and electron diffraction pattern for the same alloy in the as quenched state

Fig. 4a depicts isochronal curves of magnetic relative permeability μ_r and resistivity ρ determined at room temperature for annealed samples and plotted versus 1-h annealing

temperature T_a for the $Fe_{76}Nb_2Si_{13}B_9$ alloy. One can see that $\mu_r(T_a)$ shows a maximum at T_a=673 K while $\rho(T_a)$ strongly drops down for T_a>750 K. Permeability maximum means that 1-h annealing at a given temperature, usually denoted as T_{op} (per definition the 1-h optimization annealing temperature) causes an enhancement of soft magnetic properties. From the data presented in Fig. 4a T_{op} is found to be 673 K. A strong decrease of resistivity for higher T_a is due to crystallization of initially amorphous sample. Thus one can conclude that the observed soft magnetic enhancement effect takes place after annealing at T_{op} of about 80 K lower than the crystallization temperature. The optimized microstructure i.e. the microstructure of the $Fe_{76}Nb_2Si_{13}B_9$ samples after the 1-h optimization annealing is shown in Fig. 4b (HRTEM image) where the electron diffraction pattern is also presented. It is evident that the applied annealing does not lead to formation of any iron nanograins and the optimized microstructure corresponds to the relaxed amorphous phase.

Fig. 5a shows isochronal curves of relative magnetic permeability μ_r and resistivity ρ plotted versus 1-h annealing temperature T_a for the $Fe_{74}Cu_1Zr_3Si_{13}B_9$ alloy. One can see that in this case T_{op}=823 K and is much higher than the crystallization temperature T_{x1}=670 K corresponding to the abrupt drop of resistivity. The optimized microstructure together with the electron diffraction pattern typical for nanostructured materials are shown in Fig. 5b.

a)

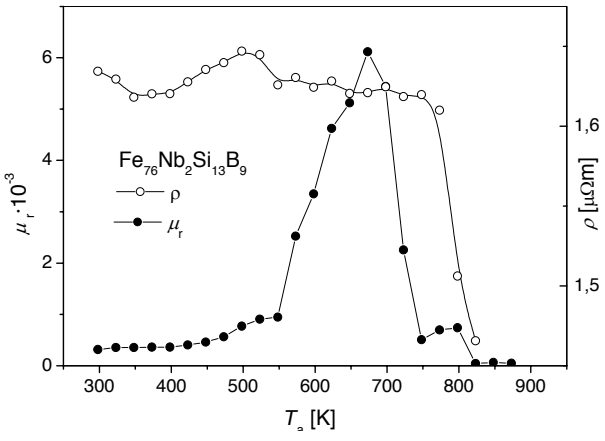

b)

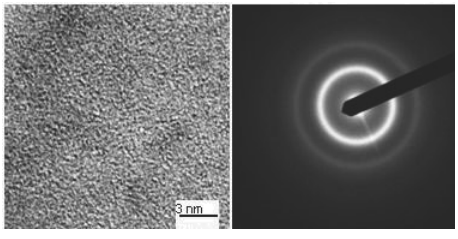

Fig. 4. a) Magnetic permeability μ_r and resistivity ρ versus 1-h annealing temperature for the $Fe_{76}Nb_2Si_{13}B_9$ alloy; b) HRTEM image for sample of the $Fe_{76}Nb_2Si_{13}B_9$ alloy annealed at T_{op}=673 K for 1 h (the optimized microstructure)

a)

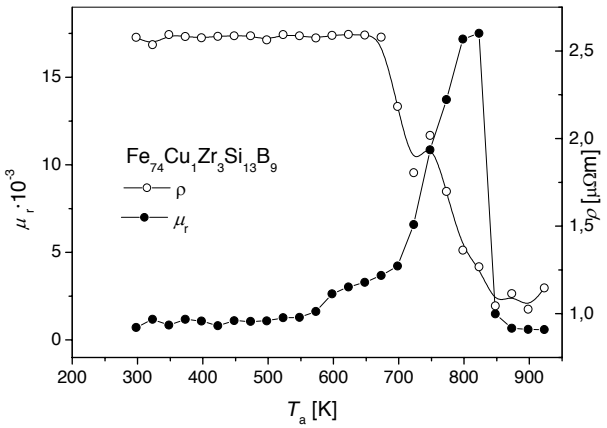

b)

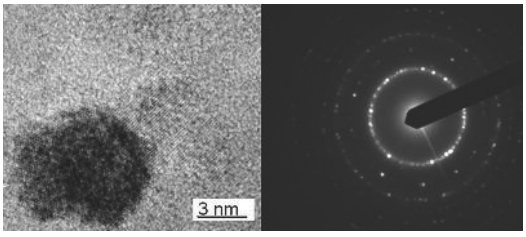

Fig. 5 a) Magnetic permeability μ_r and resistivity ρ versus 1-h annealing temperature for the $Fe_{74}Cu_1Zr_3Si_{13}B_9$ alloy; b) HRTEM image for sample of the $Fe_{74}Cu_1Zr_3Si_{13}B_9$ alloy annealed at T_{op}=823 K for 1-h (the optimized microstructure).

The influence of the optimization annealing on the magnetization process is presented in Fig. 6 where magnetic polarization $\mu_0 M$ versus magnetic field H is plotted for the $Fe_{76}Nb_2Si_{13}B_9$ alloy in the as quenched state and after the optimization annealing. One can see that the sample after the optimization annealing magnetically saturates much easier than the sample in the as quenched state.

Magnetic instabilities a characteristic feature of the as quenched state can be monitored via measuring the magnetic relaxation intensity $\Delta\mu/\mu$. Changes of this quantity with 1-h annealing temperature are depicted in Fig. 7 where $\Delta\mu/\mu$ for the $Fe_{76}Nb_2Si_{13}B_9$ and $Fe_{75.75}Ag_{0.25}Nb_2Si_{13}B_9$ alloys is plotted versus T_a. One can see that for the $Fe_{76}Nb_2Si_{13}B_9$ alloy in the as quenched state $\Delta\mu/\mu \approx 13.6$ % and increases with increasing T_a up to 400 K. At higher annealing temperatures $\Delta\mu/\mu$ continuously decreases and at T_{op} is about 6 %. For the $Fe_{75.75}Ag_{0.25}Nb_2Si_{13}B_9$ alloys the initial value of $\Delta\mu/\mu$ is about 10% and at T_{op} about 5%. It is important to state that after the optimization annealing thermal/time instabilities of amorphous alloys are significantly reduced.

Fig. 8 shows magnetostriction coefficient $\lambda_{||S}$ measured at saturation magnetic field versus 1-h annealing temperatures for the $Fe_{76}Nb_2Si_{13}B_9$ and $Fe_{74}Cu_1Zr_3Si_{13}B_9$ alloys. From this figure it can be concluded that $\lambda_{||S}$ continuously decreases with increasing annealing temperature.

Plastic deformation $\varepsilon=d/2r$ (where d is the ribbon thickness and r is the bending radius corresponding to formation of the first

brittle cracks) plotted versus 1-h annealing temperature is shown in Figs. 9 and 10 for different groups of the examined alloys. From these figures one can conclude that plastic deformation of the examined samples in the as quenched state is the highest for the $Fe_{76}Nb_2Si_{13}B_9$, $Fe_{75.75}Ag_{0.25}Nb_2B_{22}$, and $Fe_{74}Co_5Cu_1Nb_2B_{18}$ alloys. In all cases with increasing T_a a drastic decrease of ε is observed.

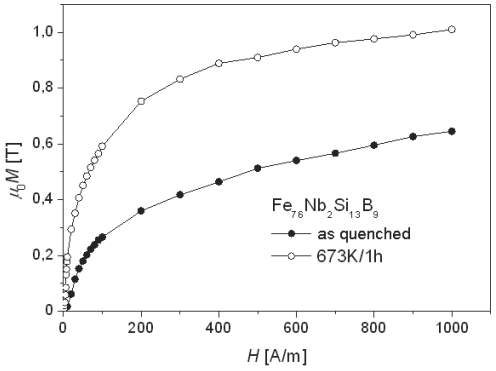

Fig. 6. Magnetization curves for the $Fe_{76}Nb_2Si_{13}B_9$ alloy In the as quenched state and after optimization annealing at T_{op}=673 K for 1-h

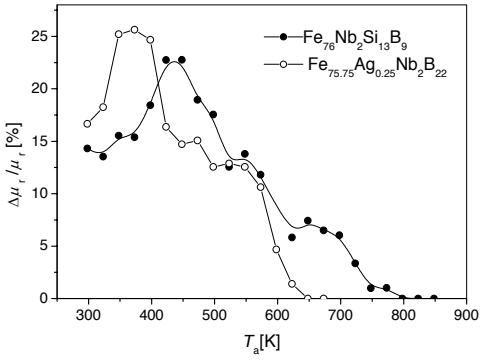

Fig. 7. Magnetic relaxation intensity $\Delta\mu_r/\mu_r$ versus 1-h annealing temperature T_a for different examined alloys

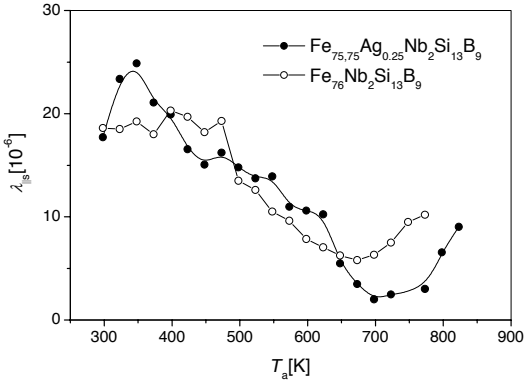

Fig. 8. Parallel magnetostriction coefficient $\lambda_{||S}$ messured at saturation magnetic field (H=0.1 T) versus 1-h annealing temperatures for two examined alloys

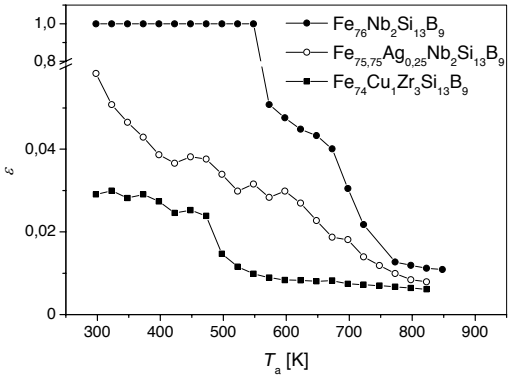

Fig. 9. Plastic deformation ε versus 1-h annealing temperature T_a for the $Fe_{76}Nb_2Si_{13}B_9$, $Fe_{75.75}Ag_{0.25}Nb_2Si_{13}B_9$ and $Fe_{74}Cu_1Zr_3Si_{13}B_9$ examined alloys

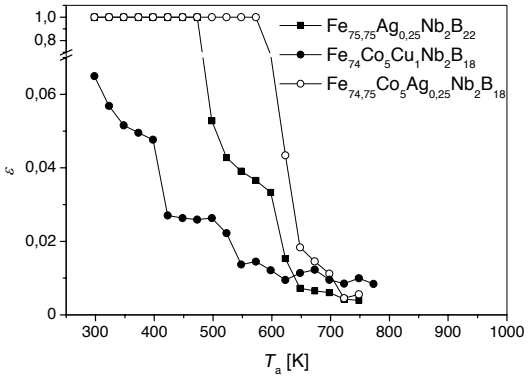

Fig. 10. Plastic deformation ε versus 1-h annealing temperature T_a for the $Fe_{75.75}Ag_{0.25}Nb_2B_{22}$, $Fe_{74}Co_5Cu_1Nb_2B_{18}$, $Fe_{74.75}Co_5Ag_{0.25}Nb_2B_{18}$ alloys

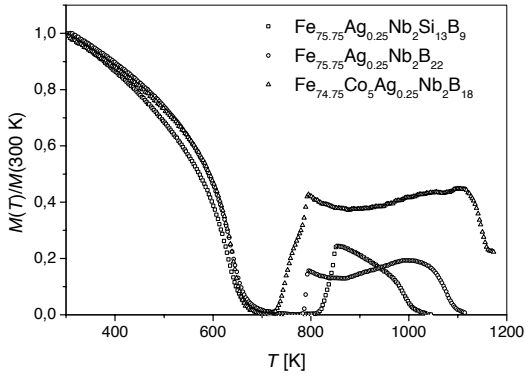

Fig. 11. Normalized magnetization in satruation ($\mu_0 H$ = 0.5 T) versus temperature for different examined alloys (heating rate 5 K/min)

Fig. 11 shows normalized magnetization in saturation ($\mu_0 H$ = 0.5 T) versus temperature determined for different examined alloys (heating rate 5 K/min). With increasing

temperature magnetization decreases up to the Curie point of the amorphous phase and at higher temperatures (i.e. for 700 K<T<750 K) the examined sample is in paramagnetic state with almost zero magnetization. At temperatures corresponding to crystallization (or nanocrystallization) an abrupt increase of magnetization due to formation of iron nanograins is observed.

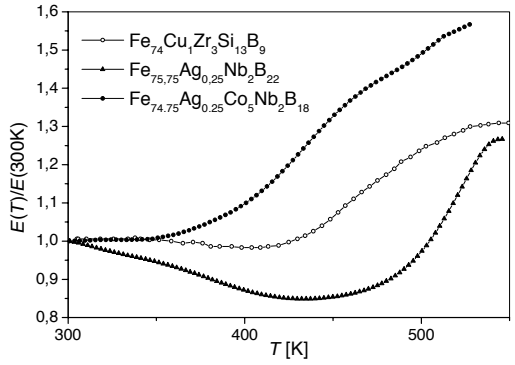

Fig. 12. Normalized Young's modulus E versus temperature for the $Fe_{74}Cu_1Zr_3Si_{13}B_9$, $Fe_{75.75}Ag_{0.25}Nb_2B_{22}$ and $Fe_{74.75}Ag_{0.25}Co_5Nb_2B_{18}$ amorphous alloys

Dependence of Young's modulus E versus temperature for the $Fe_{74}Cu_1Zr_3Si_{13}B_9$, $Fe_{75.75}Ag_{0.25}Nb_2B_{22}$ and $Fe_{74.75}Ag_{0.25}Co_5Nb_2B_{18}$ amorphous alloys is depicted in Fig. 12. One can see that E initially decreases with temperature as it should be expected for any solid state and at higher temperatures strongly increases indicating an reinforcement of interatomic interactions due to a reduction of interatomic distances in amorphous structure.

3.2. Magnetoimpedance effect

Changes of magnetoimpedance effect caused by 1-h annealing at different temperatures T_a, determined at frequency 1 MHz, are shown in Figs. 13 and 14 for contact and non-contact method, respectively. One can see that in any case $(\Delta Z/Z)_{max}$ shows a maximum positioned at the 1-h optimization annealing temperature T_{op} - similar to the permeability maxima $\mu_i(T_a)$. According to Fig. 13 for all examined alloys in the as quenched state $(\Delta Z/Z)^{cq}{}_{max}$ is relatively low i.e. $(\Delta Z/Z)^{cq}{}_{max} \approx$ 4-7%. Annealing at T_{op} causes a strong increase of this quantity - e.g., twice for the $Fe_{75.75}Ag_{0.25}Nb_2Si_{13}B_9$ alloy or even a 6 times for the $Fe_{74}Cu_1Zr_3Si_{13}B_9$ alloy.

In general, according to Figs. 13 and 14 the observed magnetoimpedance effect measured by applying non-contact method is much higher than this one measured by contact method. In some cases it can be even two orders of magnitude. For example in the as quenched state $(\Delta Z/Z)^{nc,q}{}_{max}$ is about 350% - 600% ($(\Delta Z/Z)^{c,q}{}_{max} \approx$ 4-7%.) and after annealing at T_{op} $(\Delta Z/Z)^{nc,op}{}_{max}$ is of the order of 10000% (e.g. for the $Fe_{74}Cu_1Zr_3Si_{13}B_9$ alloy).

The dependence of non-contact magnetoimpedance effect on static magnetic field H_{dc} is presented in Fig. 15 for the $Fe_{75.75}Ag_{0.25}Nb_2Si_{13}B_9$ alloy in the as quenched state and after the 1-h optimization annealing (698 K/1h). One can see that the highest values of $(\Delta Z/Z)$ are at relatively weak magnetic fields. Moreover the 1-h optimization annealing causes an increase of the $(\Delta Z/Z)^{nc}{}_{max}$ from 450% to 7000%.

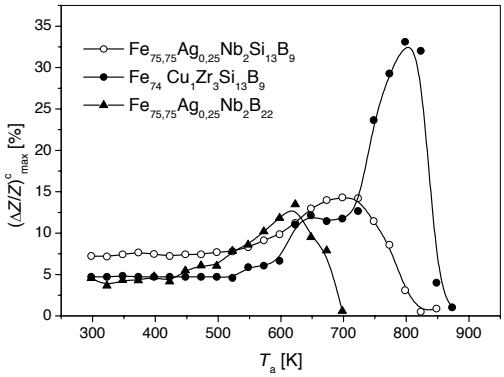

Fig. 13. Contact magnetoimpedance effect $(\Delta Z/Z)^{c}{}_{max}$ versus 1-h annealing temperature T_a for different examined alloys (frequency 1 Mz).

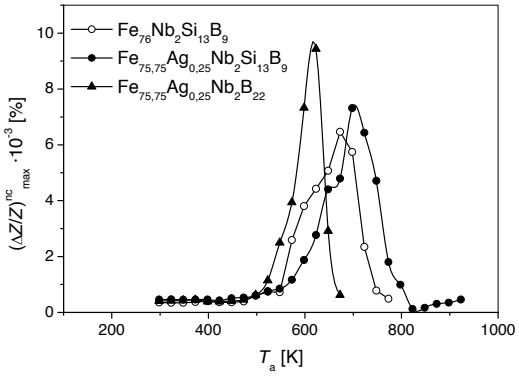

Fig. 14. Non-contact magnetoimpedance effect $(\Delta Z/Z)^{nc}{}_{max}$ plotted versus 1-h annealing temperature T_a for different examined alloys (frequency 1 Mz)

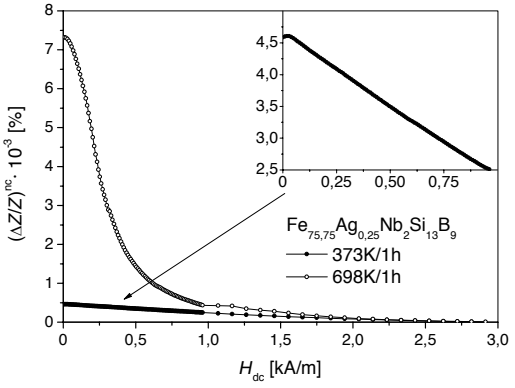

Fig. 15. Non-contact magnetoimpedance effect $(\Delta Z/Z)^{nc}$ versus static magnetic field H_{dc} for the $Fe_{74}Cu_1Zr_3Si_{13}B_9$ alloy in the as quenched state and after the 1-h optimization annealing 698 K/1h (frequency 1 Mz); in the inset $(\Delta Z/Z)^{nc}$ for the as quenched state is reploted

Sensitivity of the magnetoimpedance effect measured by making use of the non-contact method (defined by equation (3)) for two amorphous alloys i.e. for the $Fe_{74}Cu_1Zr_3Si_{13}B_9$ and $Fe_{75.75}Ag_{0.25}Nb_2B_{22}$ alloys is shown in Fig. 16.

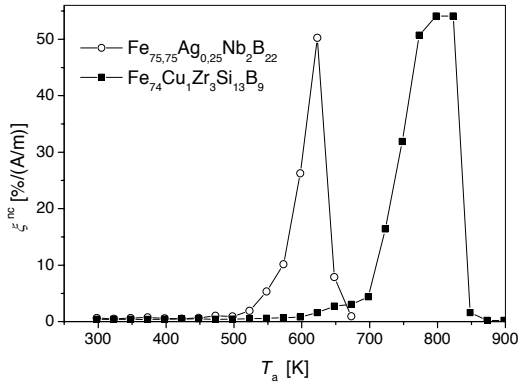

Fig. 16. Sensitivity of non-contact magnetoimpedance effect ζ^{nc} (defined by equation (3)) versus 1-h annealing temperature T_a for two amorphous alloys $Fe_{74}Cu_1Zr_3Si_{13}B_9$ and $Fe_{75.75}Ag_{0.25}Nb_2B_{22}$

In the as quenched state ζ^{nc} values are rather small i.e. ζ^{nc} =0.4% A/m and 0.7% A/m for the $Fe_{75.75}Ag_{0.25}Nb_2B_{22}$ and $Fe_{74}Cu_1Zr_3Si_{13}B_9$ alloy, respectively. According to Fig. 16 the sensitivity factor drastically increases after the optimization annealing reaching values of about 15% A/m and 54% A/m, respectively.

Variation of magnetoimpedance effect with frequency determined by making use of non-contact method for different examined alloys is presented in Figs. 17 and 18.

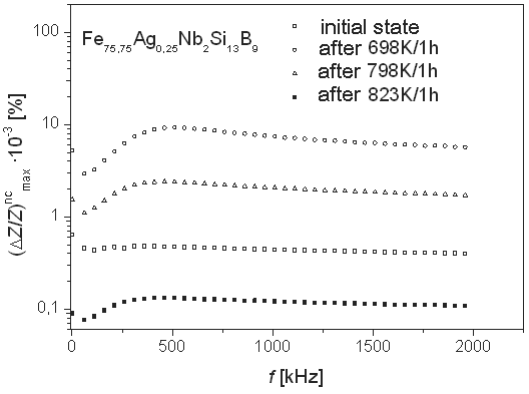

Fig. 17. Non-contact magnetoimpedance effect $(\Delta Z/Z)^{nc}{}_{max}$ versus frequency f for the $Fe_{75.75}Ag_{0.25}Nb_2Si_{13}B_9$ alloy after different annealing

One can see that in all examined cases a broad maximum at about 450 kHz is observed. In the frequency range from 50 kHz to 2 MHz all examined alloys show a giant magnetoimpedance effect of the order of 10^4%. It has to be stressed that at frequency $f > 700$ kHz magnetoimpedance effect is practically frequency independent.

All the characteristic parameters determined for the examined alloys in the as quenched state and after the 1-h optimization annealing are listed in Table 1.

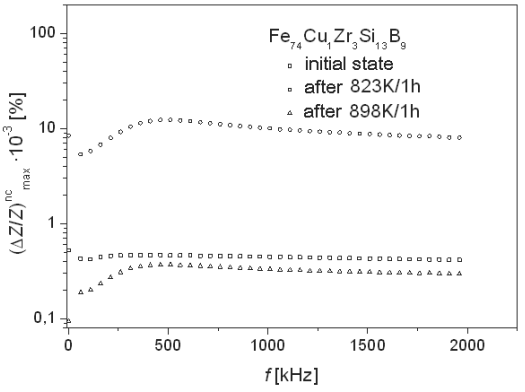

Fig. 18. Non-contact magnetoimpedance effect $(\Delta Z/Z)^{nc}{}_{max}$ versus frequency f for the $Fe_{74}Cu_1Zr_3Si_{13}B_9$ alloy after different annealing

4. Discussion

Based on the data listed in Table 1 one can state that magnetic permeability of the examined amorphous alloys in the as quenched state is comparable to that of classical silicon steel. In spite of this amorphous alloys show higher resistivity ensuring lower eddy current losses. The Curie temperatures (about 600 K) are lower than that for silicon steel but high enough for different applications. The main disadvantage of amorphous material consists in thermal/time instabilities of their physical properties. Indeed, during fabrication due to fast cooling from liquid phase a relatively high content of free volume is frozen into material. So, at room temperature amorphous alloys are not in thermodynamic equilibrium and tend to equilibrium via the so-called structural relaxation and crystallization [20,23,28]. These two processes are diffusion controlled and essentially are responsible for thermal/time instabilities of different physical properties.

In many papers it was shown that in soft magnetic amorphous alloys obtained by melt spinning a change of free volume content is strictly correlated with the intensity of magnetic relaxation $\Delta\mu_r/\mu_r$ determined in weak magnetic fields [23,28,29]. A successive annealing out of free volume due to preliminary thermal annealing of amorphous alloys is well demonstrated in Fig. 7 for the $Fe_{76}Nb_2Si_{13}B_9$ and $Fe_{75.75}Ag_{0.25}Nb_2Si_{13}B_9$ alloys. From this figure one can see that $\Delta\mu_r/\mu_r$ initially increases which can be explained by coagulation of free volume and for higher annealing temperatures continuously decreases indicating a partial disappearance of magnetic instabilities. Free volume annealing out effect is also observed in Fig. 12 via temperature dependences of Young's modulus E. It is evident that the observed increase in E is due to a decrease of interatomic distances in amorphous structure. Similar effect was observed in [30] where the increase of E in amorphous alloys was also attributed to annealing out of free volume.

Table 1.
Different physical quantity determined for the examined amorphous alloys in the as quenched state and after the 1-h optimization annealing (index op) - T_C = Curie temperature, T_{op} = 1-h optimization annealing temperature, T_{x1} = first stage crystallization temperature, μ_r = magnetic permeability, $\Delta\mu_r/\mu_r$ = intensity of magnetic relaxation, $\Delta Z/Z$ = magnetoimpedance effect, ξ = magnetoimpedance sensitivity, ρ = resistivity, $\lambda_{||S}$ = magnetostriction coefficient, ε = plastic deformation, δ = penetration depth. The alloys notation is the following: A – $Fe_{76}Nb_2Si_{13}B_9$, B – $Fe_{75.75}Ag_{0.25}Nb_2Si_{13}B_9$, C – $Fe_{74}Cu_1Zr_3Si_{13}B_9$, D – $Fe_{75.75}Ag_{0.25}Nb_2B_{22}$, E – $Fe_{74}Co_5Cu_1Nb_2B_{18}$, F – $Fe_{74.75}Co_5Ag_{0.25}Nb_2B_{18}$

Measured quantity	Alloy					
	A	B	C	D	E	F
T_c, K	635	626	590	636	630	638
T_{op}, K	673	698	823	623	623	598
T_{x1}, K	784	780	710	742	610	675
μ^q_r	350	510	720	420	715	500
μ^{op}_r	6100	4550	17500	7400	3100	4400
$(\Delta\mu_r/\mu_r)^q$, %	13.6	10.0	8	16.7	17.0	13.0
$(\Delta\mu_r/\mu_r)^{op}$, %	6.1	4.9	1	1.4	3.1	2.3
$(\Delta Z/Z)^{c,q}_{max}$, %	6	7	5	5	6	4
$(\Delta Z/Z)^{c,op}_{max}$, %	14	14	32	13	10	11
$(\Delta Z/Z)^{nc,q}_{max}$, %	350	450	400	400	600	500
$(\Delta Z/Z)^{nc,op}_{max}$, %	6470	6430	10000	9430	5100	6350
$\xi^{nc,q}$,%/(A/m)	0.6	0.4	0.4	0.6	0.7	0.7
$\xi^{nc,op}$,%/(A/m)	40	28	54	50	14	36
ρ^q, μΩm	1.63	1.72	2.51	1.62	1.68	1.86
ρ^{op}, μΩm	1.62	1.75	1.25	1.60	1.62	1.88
$\lambda^q_{||S} \cdot 10^6$	18.6	17.7	19.6	12.4	20.5	20.4
$\lambda^{op}_{||S} \cdot 10^6$	5.8	2.0	0.5	2.8	7.2	5.2
ε^q	1	0.06	0.03	1	0.065	1
ε^{op}	0.020	0.018	0.008	0.015	0.01	0.093
$2 \cdot \delta^{op}$, μm	11.6	19.96	6	10.5	15.66	14.66
T_{op}/1h	RA*	RA*	RA+N*	RA*	RA+N*	RA*

* The optimized microstructure, RA - relaxed amorphous phase, N - nanocrystalline phase

The process of decreasing free volume content in a natural way leads to: i) formation of small iron clusters magnetically coupled in different manner [31], ii) a reduction of internal stresses and iii) a reduction of the stabilization energy of magnetic domain wall system [32]. The data presented in Fig. 8 shows also that the parallel magnetostriction coefficient $\lambda_{||S}$ is very sensitive to local structural changes in amorphous structure. This is a simple consequence of the fact that $\lambda_{||S}$ is proportional to correlation functions of magnetic moments short range in nature [33]. A decrease of $\lambda_{||S}$ means obviously a decrease of magnetoelastic energy one of the important factors in magnetic materials.

The data listed in Table 1 shows that Ag as an alloying addition in the $Fe_{76}Nb_2Si_{13}B_9$ base alloy practically does not change the initial free volume content (magnetic relaxation).

In contrast to this, zirconium as an alloying addition causes a reduction of the initial free volume content. This effect one can explain based on the metal melting model which predicts that free volume content frozen into amorphous material is irreversibly proportional to the melting temperature of the alloying addition [34].

According to the results presented in Figs. 4 and 5 in all examined alloys the enhancement of magnetic permeability effect is observed. Indeed, after the 1-h optimization annealing at temperatures T_{op} (see Table 1) permeability increases more than 20 times giving magnetic material much better than classical silicon steel. Fig. 4b shows also that in the case of the $Fe_{76}Nb_2Si_{13}B_9$ alloy the optimized microstructure (after 1-h annealing at T_{op}=673 K) is free of iron nanograins i.e. corresponds to relaxed amorphous phase. In contrast to this the optimized microstructure of the $Fe_{74}Cu_1Zr_3Si_{13}B_9$ alloy 1-h annealed at T_{op} = 823 K corresponds to nanostructural phase.

From practical point of view it is clear that the considered alloy after the optimization annealing should show as high as possibly

plastic deformation. The evolution of plastic deformation with 1-h annealing temperature is presented in Figs. 9 and 10. It is evident that for the following alloys $Fe_{76}Nb_2Si_{13}B_9$, $Fe_{75,75}Ag_{0,25}Nb_2Si_{13}B_9$, $Fe_{75,75}Ag_{0,25}Nb_2B_{22}$, and $Fe_{74,75}Co_5Ag_{0,25}Nb_2B_{18}$ for which the optimized microstructure corresponds to the relaxed amorphous phase the plastic deformation is much higher than for the $Fe_{74}Cu_1Zr_3Si_{13}B_9$ and $Fe_{74}Co_5Cu_1Nb_2B_{18}$ alloys for which the optimized microstructure contains iron nanograins. This fact is in agreement with similar examinations carried out for different amorphous alloys [23,31,35,36].

In general, the observed enhancement of magnetic permeability effect is due to averaging out magnetic anisotropy in magnetic materials [37]. It was already mentioned that in amorphous alloys for which the optimized misrostructure is free of iron nanocrystallites additional effects should be taken into account: i) annealing out of free volumes leading to formation of small iron clusters, ii) reduction of internal stresses, iii) reduction of magnetostriction coefficient, iv) reduction of stabilization energy and v) increase of magnetic polarization.

Taking into account the factors listed above one can express magnetic permeability μ_r as:

$$\mu_r(T,t) \approx J_S^2 \left\{ \mu_0 \left[K_{am}^4 \left(\frac{D_{am}}{\sqrt{A_{am}}} \right)^6 + \frac{3}{2}\lambda_S \sigma + (w^2 c/3k_B T)\left(1 - exp\left(-\frac{t}{\tau}\right)\right) \right] \right\}^{-1} \quad (4)$$

and for a material containing nanocrystalline phase one can get:

$$\mu_r(T,t) \approx J_S^2 \left\{ \mu_0 \left[\alpha^4 K_1^4 D^6 \left(\frac{1}{\sqrt{A_{cr}}} + \frac{\alpha^{-\frac{1}{3}} - 1}{\sqrt{A_{am}}} \right)^6 + \frac{3}{2}\lambda_S + (w^2 c/3k_B T)\left(1 - exp\left(-\frac{t}{\tau}\right)\right) \right] \right\}^{-1} \quad (5)$$

where J_S is the magnetic polarization in saturation, α is the volume fraction of nanocrystalline phase, D_{am} is the mean dimension of magnetic clusters in amorphous phase (regions with correlated magnetic moments), K_{am} is the anisotropy constant of amorphous phase, D is the mean grainsize, K_1 - is the anisotropy constant of nanocrystalline phase, λ_S - magnetostriction coefficient, A_{cr} and A_{am} are constant of exchange interaction for crystalline phase and amorphous phase, respectively, w is the Neel energy of interaction of magnetization and relaxators, c is the relaxatores content, k_B is the Boltzmann constant, τ is the relaxation time and t is the time after demagnetization.

According to the results presented in Figs. 13 and 14 magnetoimpedance effect mainly depends on magnetic permeability value. One can see that $\Delta Z/Z$ versus T_a shows maxima at temperatures T_{op} which means that the models explaining the soft magnetic properties enhancement effect thereby explain also ($\Delta Z/Z$) maxima. This is presented in Fig. 19 where non-contact magnetoimpedance effect $(\Delta Z/Z)^{nc}_{max}$ and μ_r are plotted versus 1-h annealing temperature T_a for the $Fe_{75,75}Ag_{0,25}Nb_2B_{22}$ alloy.

It is proper to add that for all examined alloys after 1-h annealing at T_{op} ($\Delta Z/Z$) increases at least a few times (see Table 1). It can be shown that for such melt spun ribbons with relatively high resistivity (1-2 μΩm) and thickness of the order of 20 μm magnetic field penetration distance for frequency 1 MHz is comparable with the sample thickness. Moreover, for an open magnetic circuit in the case in which imaginary part of complex permeability is negligible in relation to the real one the magnetoimpedance effect can be expressed as:

$$\left(\Delta Z/Z\right)^{nc} \approx \left[\frac{\mu_r(H_{dc}, f, \rho, N, J) - \mu_r(H_{dc,max}, f, \rho, N, J)}{\mu_r(H_{dc,max}, f, \rho, N, J)} \right] \quad (6)$$

where f is the frequency of measurement magnetic field and N is the demagnetization factor. From equation (6) it is clear that magnetoimpedance effect in examined alloys is mainly determined by the ratio $\mu(H_{dc})/\mu(H_{dc\ max})$. In particular, a constant value of non-contact magnetoimpedance effect in the frequency range from 50 kHz to 2 MHz show that this ratio does not change with frequency.

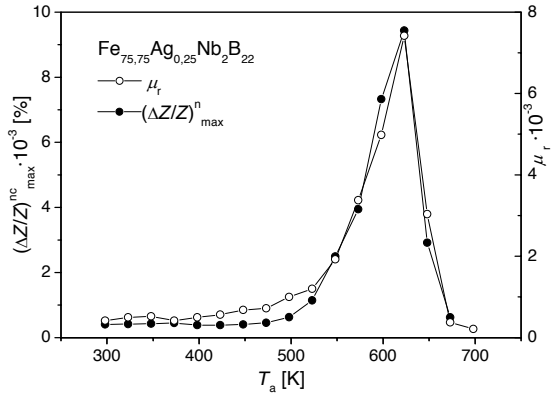

Fig. 19. Non-contact magnetoimpedance effect $(\Delta Z/Z)^{nc}_{max}$ and magnetic permeability μ_r versus 1-h annealing temperature T_a for the $Fe_{75.75}Ag_{0.25}Nb_2B_{22}$ alloy

5. Conclusions

The main conclusions of the present paper can be summarized as follows:

- Soft magnetic properties of the examined alloys based on iron can be enhanced by applying a suitable 1-h annealing at temperatures T_{op} listed in Table 1. After annealing at this characteristic temperature magnetic permeability in relation to the as quenched state increases more than 20 times and non-contact magnetoimpedance effect $(\Delta Z/Z)^{nc}_{max}$ is of the order of 10^4%.
- The observed enhancement effect can be explained based on the random anisotropy model supplemented by terms describing magnetoelastic energy and stabilization energy related to free volume content.
- For the alloys for which the optimized microstructure corresponds to the relaxed amorphous the plastic deformation corresponding to formation of brittle cracks is much higher than for nanostructured alloys.
- In the frequency range from 700 kHz to 2 MHz $(\Delta Z/Z)^{nc}_{max}$ is approximately constant (see Figs. 17 and 18).
- In the examined group of alloys the best candidate for magnetoimpedance sensor application is the $Fe_{75,75}Ag_{0,25}Nb_2B_{22}$ alloy for which $(\Delta Z/Z)^{nc}_{max} \approx 10^4$%, $\varepsilon^{op} = 0.015$.

References

[1] L.A. Dobrzański, M. Drak, Hard magnetic composite materials Nd-Fe-B with additions of iron and X2CrNiMo-17-12-2 steel, Journal of Alloys and Compounds 449/1-2 (2008) 88-92.

[2] R. Hasegawa, Advances in amorphous and nanocrystalline magnetic materials, Journal of Magnetism and Magnetic Materials 304 (2006) 187-191.

[3] B. Tomczuk, D. Koteras, Magnetic flux distribution in the amorphous modular transformers, Journal of Magnetism and Magnetic Materials 323 (2011) 1611-1615.

[4] G. Haneczok, R. Wroczyński, P. Kwapuliński, A. Chrobak, Z. Stokłosa, J. Rasek, Electro/magnetic shielding effectiveness of soft magnetic Fe80Nb6B14 amorphous alloy, Journal of Materials Processing Technology 209 (2009) 2356-2360.

[5] A. Chrobak, A. Kaleta, P. Kwapuliński, M. Kubisztal, G. Haneczok, Magnetic shielding effectiveness of iron-based amorphous alloys and nanocrystalline composites, Proceedings of the International Conference on Soft Magnetic Materials, SMM'20, IEEE Transactions on Magnetics, doi: 10.1109/TMAG.2011.2172587, Greece, 2011.

[6] Manh-Huong Phan, Hua-Xin Peng, Giant magneto-impedance materials: Fundamentals and applications, Progress in Materials Science 53 (2008) 323-420.

[7] L. Kraus, Off-diagonal magnetoimpedance in stress-annealed amorphous ribbons Journal of Magnetism and Magnetic Materials 320 (2008) 746-749.

[8] M. Kuźmiński, K. Nesteruk, H.K. Lachowicz, Magnetic field meter based on giant magnetoimpedance effect, Sensors and ActuatorsA 141 (2008) 68-75.

[9] S.N. Kane, A. Gupta, T. Kulik, L. Kraus, Influence of intrinsic and induced anisotropy on magnetoimpedance effect in amorphous Co67Fe4Mo1.5Si16.5B11, Journal of Magnetism and Magnetic Materials 254-255 (2003) 498-500.

[10] S. Dwevedi, G. Markandeyulu, P.R. Ohodnicki, A. Leary, M.E. McHenry, Stress-MI and domain studies in Co-based nanocrystalline ribbons, Journal of Magnetism and Magnetic Materials 323 (2011) 1929-1933.

[11] N.A. Buznikov, A.S. Antonov, A.A. Rakhmanov, A model for torsion-stress effect on nonlinear magnetoimpedance in amorphous wires with negative magnetostriction, Journal of Magnetism and Magnetic Materials 323 (2011) 190-195.

[12] Yu Geliang, Bu Xiongzhu, Xiang Chao, Xu Hong, Design of a GMI magnetic sensor based on longitudinal excitation, Sensors and Actuators A 161 (2010) 72-77.

[13] Sheikh Manjura Hoque, A.K.M. Rezaul Haque, Md. Obaidur Rahman, N. H. Nghi, M.A. Hakim, Shireen Akhter, Ultra-soft magnetic properties and giant magneto-impedance of Co68Fe4.5Si12.5B15, Journal of Non-Crystalline Solids 357 (2011) 2109-2114.

[14] G. Haneczok, P. Kwapuliński, Z. Stokłosa, J. Rasek, R. Wroczyński, Archives of Materials Science 4 (2003) 373-391.

[15] F.X. Qin, H.X. Peng, V.V. Popov, M.H. Phan, Giant magneto-impedance and stress-impedance effects of microwire composites for sensing applications, Solid State Communications 151 (2011) 293-296.

[16] P. Delooze, L.V. Panina, D.J. Mapps, K. Ueno, H. Sano, Effect of transverse magnetic field on thin-film magneto impedance and application to magnetic recording, Journal of Magnetism and Magnetic Materials 272-276 (2004) 2266-2268.

[17] Lei Chen, Chen-Chen Bao, Hao Yanga, Ding Li, Chong Lei, Tao Wang, Heng-Yao Hu, Meng He, Yong Zhou, Da-Xiang Cui, A prototype of giant magnetoimpedance-based biosensing system for targeted detection of gastric cancer cells, Biosensors and Bioelectronics 26 (2011) 3246-3253.

[18] A.T. Le, N.Q. Hoa, P.D. Tam, D.G. Park, M.H. Phan, H. Srikanth, S.C. Yu, Enhancement of the giant magnetoimpedance effect and its magnetic response in ion-irradiated magnetic amorphous ribbons, Materials Science and Engineering B 166 (2010) 89-93.

[19] S. Dwevedi, G. Sreenivasulu, G. Markandeyulu, Contact and non-contact magnetoimpedance in amorphous and nanocrystalline Fe73.5Si13.5B8CuV3Al ribbons, Journal of Magnetism and Magnetic Materials 322 (2010) 311-314.

[20] A. Chrobak, D. Chrobak, G. Haneczok, P. Kwapuliński, Z. Kwolek, M. Karolus, Influence of Nb on the first stage of crystallization in the Fe86-xNbxB14 amorphous alloys, Materials Science and Engineering A 382 (2004) 401-406.

[21] D. Szewieczek, J. Tyrlik-Held, S. Lesz, Structure and mechanical properties of amorphous Fe84Nb7B9 alloy during crystallization, Journal of Achievements in Materials and Manufacturing Engineering 24 (2007) 87-90.

[22] P. Kwapulinski, Z. Stokłosa, J. Rasek, G. Badura, G. Haneczok, L. Pajak, J. Lelątko, Influence of alloying additions and annealing time on magnetic properties in amorphous alloys based on iron, Journal of Magnetism and Magnetic Materials 320 (2008) 778-782.

[23] Z. Stokłosa, P. Kwapuliński, J. Rasek, G. Badura, G. Haneczok, L. Pająk A. Kolano-Burian, Optimization of soft magnetic properties and crystallization in FeAgNbSiB, FeAgNbB and FeAgCoNbB amorphous alloys, Journal of Alloys and Compounds 507 (2010) 465-469.

[24] P. Kwapuliński, J. Rasek, Z. Stokłosa, G. Badura, B. Kostrubiec, G. Haneczok, Magnetic and mechanical properties In FeXSiB (X=Cu, Zr, Co) amorphous alloys, Archives of Materials Science and Engineering 31 (2008) 25-28.

[25] S. Flohrer, G. Herzer, Random and uniform anisotropy in soft magnetic nanocrystalline alloys, Journal of Magnetism and Magnetic Materials 322 (2010) 1511-1514.

[26] A. Chrobak, G. Haneczok, P. Kwapuliński, D. Chrobak, Z. Stokłosa, J. Rasek, Soft magnetic properties of the Fe72Co10Nb6B12 amorphous alloy, Journal of Alloys and Compounds 423 (2006) 77-80.

[27] T. Naohara, The role of metallic (M) elements in the ageing behavior of amorphous FeSiBM (M = Nb, Zr, or V) alloys, Acta materialia 46 (1998) 4601-4607.

[28] P. Kwapuliński, J. Rasek, Z. Stokłosa, G. Haneczok, Magnetic properties of amorphous and nanocrystalline alloys based on iron, Journal of Materials Processing Technology 157-158 (2004) 735-742.

[29] P. Kwapuliński, Z. Stokłosa, A. Chrobak, J. Rasek, G. Haneczok, Optimisation of soft magnetic properties in Fe-B and Fe-B-Si amorphous alloys obtained by melt spinning method, Acta Physica Polonica A 102 (2002) 309-316.

[30] P. Kwapuliński, A. Chrobak, G. Haneczok, Z. Stokłosa, J. Rasek, Structural relaxation In Fe86-xNbxB14amorphous alloys, Journal of Magnetism and Magnetic Materials 304 (2006) 654-656.
[31] G. Haneczok, J.E. Frąckowiak, A. Chrobak, P. Kwapuliński, J. Rasek, Magnetic permeability enhancement effect in the Fe86-xNbxB14 (x = 5, 6) amorphous alloys, Physica Status Solidi a 202 (2005) 2574-2581.
[32] H. Kronmüller, Theory of the coercive field in amorphous ferromagnetic alloys, Journal of Magnetism and Magnetic Materials 24 (1981) 159-167.
[33] G Haneczok, Ł Madej, A Chrobak, P Kwapuliński, Z Stokłosa, J Rasek, Influence of free volume on magnetoelastic coupling in iron-based amorphous alloys, Physica Scripta, 81 (2010) 025702.
[34] T. Górecki, Cz. Górecki, K. Książek, S. Wacke, Effective vacancy formation energy and the solute - vacancy binding energy in binary Cu - based alloys, Visnyk of the Lviv University, Series Khimichna 48/1 (2007) 88-94.
[35] L. Pešek, L.A. Dobrzański, P. Zubko, J. Konieczny, Mechanical properties of metallic ribbons investigated by depth sensing indentation technique, Journal of Magnetism and Magnetic Materials 304 (2006) 645-647.
[36] J. Konieczny, L.A. Dobrzański, L. Pešek, P. Zubko, Mechanical properties of Co based amorphous ribbons Journal of Achievements in Materials and Manufacturing Engineering 31 (2008) 254-261.
[37] K. Suzuki, J.M. Cadogan, Random magnetocrystalline anisotropy in two-phase nanocrystalline systems, Physical Review B 58 (1998) 2730.